Contents list available at IJRED website

Int. Journal of Renewable Energy Development (IJRED)

Journal homepage: http://ejournal.undip.ac.id/index.php/ijred

Research Article

Monitoring the Performances of a Maximum Power Point Tracking Photovoltaic (MPPT PV) Pumping System Driven by A Brushless Direct Current (BLDC) Motor

Abdellahi Ba[a,b], Mohamed El Mamy Mohamed Mahmoud[a], Ne Ould Dah[a], Diakité Amadou[a], Aroudam El Hassen[b] and Chighali Ehssein[a,*]

[a]*Unité de Recherche en Electromécanique, Institut Supérieur d'Enseignement Technologique (ISET), Rossso, Mauritania*

[b]*Modeling and simulation of Mechanical Systems Laboratory, Faculty of Sciences, University Abdelmalek Essaadi, Tétouan, Morocco*

ABSTRACT. Nowadays, water pumping systems powered by solar-cell generators are one of the most important applications. It's a promising alternative to conventional electricity and diesel based pumping systems, especially for applications like community water supplies and irrigation. This study presents a monitored standalone photovoltaic solar direct pumping system using the Maximum Power Point Tracking (MPPT) algorithm to optimize the solar photovoltaic conversion efficiency. It was done at ISET-Rosso in Mauritania. The experimental setup based on Lorentz PS1200C-SJ8-5 pumping system consists of four photovoltaic (PV) panels, inverter PS1200, BLDC motor, centrifugal pump and a storage tank. The system has been monitored, in order to determine the relationship between: the DC power produced by the PV generator and the solar radiation; the water flow and the DC power and by then the relationship between the water flow and the solar radiation. The effect of ambient temperature and solar radiation on the PV panels was also done under Matlab/Simulink environment and compared to the experimental results.

Keywords: Photovoltaic, PV pumping, MPPT algorithm, BLDC motor, Monitoring

Article History: Received: May 28, 2018; Revised: January 16, 2019; Accepted: May 18, 2019; Available online: July 15, 2019
How to Cite This Article: Ba, A., Mahmoud, M.E.M, Dah, N.O., Amadou, D., El Hassen, A. and Ehssein, C. (2019) Monitoring the Performances of a Maximum Power Point Tracking Photovoltaic (MPPT PV) Pumping System Driven by A Brushless Direct Current (BLDC) Motor. International Journal of Renewable Energy Development, 8(2), 193-201.
https://doi.org/10.14710/ijred.8.2.193-201

1. Introduction

In Mauritania, there is much land but few people, in many places power is not easy to attain. In 2013, the national rate of access to electricity is estimated to be 34%. In the urban zone the rate is 58% in average while in the rural zone the rate is only 5% (Mustapha et al, 2015). To ensure the need of water, especially for rural areas and small communities, standalone photovoltaic pump systems have emerged as a result. They are commonly used in domestic and livestock water supplies and small-scale irrigation systems, especially those employed for water and energy conservation such as low head drip irrigation systems. Their main advantages over combustion engine pumps include practically zero maintenance, a long useful life, no fuel required for operation, no air contamination, and straightforward installation. Their principal disadvantage is a high capital cost. The high cost of such application and the low return on investment are constraints that holdup the popularization of bringing independent photovoltaic pumping system to large rural area.

A literature review of the widespread propagation of solar water pumping systems and technology is well presented by (Chandel et al, 2015). Several types of pumps and motors are available on the PV pumping market. The most commonly employed pump type is the centrifugal pump. Single-stage centrifugal pump are frequently used in PV shallow water pumping for low head applications. For PV subterranean water pumping and surface water pumping with higher heads, multistage centrifugal pumps are more suitable. Other pump types such as progressive cavity pumps (Lawrance & Langridge 1995) and piston pumps (Whitfield, Bentley & Burton 1995) have also been utilized.

The most commonly utilized motor type with PV pumping systems is the permanent magnet (PM) brushed dc motor Suehrcke, Appelbaum, & Reshef (1997); Surendra & Subbaraman (2002); Hadi, Tokuda & Rahardjo (2003); Akbaba (2006); Hadj Arab, Benghanem & Chenlo (2006). Other brushed dc motors such as series shunt and separately exited motors have also been investigated Koner (1995); Fam & Balachander (1988); Atlam & Kuyumcu (2003). In bore-hole and deep-well

* Corresponding author : ehssein@yahoo.fr

pumping applications, induction motors Taha & Suresh (1996); Feraga & Bouldjedri (2016) and brushless dc motors Lawrance & Langridge, (1995); Jain, Sarkar & Siddique (2015) are preferred since they require less maintenance. Other types of motors have also been used including single-phase induction motors and switched reluctance motors Metwally & Anis (1995); Vongmanee (2004).

The least expensive method of pumping water using PV energy is directly connecting a DC motor-pump set to a PV array without batteries. The theory of direct coupling between DC motors and PV units is well documented in the literature Appelbaum & Bany, (1979); Roger, (1979); Abidin & Yesilata (2004). For a given solar radiation incident on the modules and a given cell temperature, there is a unique point in the current-voltage (I-V) curve of the PV array at which the electrical power output is maximum; the maximum power point (MPP). Most DC motors can operate far from the MPP at most radiation levels and temperatures Elgendy, Zahawi & Atkinson, (2010). The point on the I-V curve where the system is operating (operating point) is determined by the intersection of the PV module I-V curve and the load I-V curve. Thus, an electrical mismatching could occur between the I-V characteristics of the motor and the I-V characteristics of the PV array.

A battery-buffered PV pumping system, where a battery is connected across the PV array and the DC motor through a voltage regulator will minimize this problem. Another possibility is to consider a maximum power point tracker (MPPT). In this case a DC-DC converter continuously matches the MPP characteristics of the PV array to the input characteristics of the DC motor that drives the pump (Calais & Hinz, 1998). The two options however, add more cost and complexity to the system and therefore, the trade between higher energy conversion efficiency and higher installation costs must be assessed.

The principal aim of this work is to suggest how the successful operation of MPPT PV pumping system based on a BLDC motor can be achieved under local working conditions.

2. Experimental Setup

The experimental setup developed and used in this study consists of two major parts: The first part of this work is devoted to setup the pumping system designed to feed a low pressure drip irrigation network; the second part is dedicated to the monitoring system.

The pumping system is composed of four Astropower photovoltaic modules (1,58x0,82m each) connected in series, Lorentz ps1200 c-sj8-5 pumping system and a storage tank. The PV panel parameters are shown in table 1. They are rated at 1000 W/m² and 25°C (STC conditions).

Table 1
Astropower model AP 190

Parameters	Value
Rated power	190 watt
Rated voltage	25,8V
Rated current	7,36A
Open circuit voltage	32,3V
Short circuit current	8,18A

The Lorentz ps1200 c-sj8-5 used includes a multistage centrifugal pump, sensorless PM BLDC motor and a controller. Their performances are shown in Table 2. This study was performed at the Higher Institute of Technological Teaching (ISET-Rosso) in Rosso-Mauritania: 16°30 North latitude, 15°48 West longitude at 8m altitude above the sea level.

Table 2
Controller performances

Parameters	Value
Item #	1222
Lift [m]	0-40m
max. flow rate [m3/h]	7.5
Max. efficiency [%]	48
PVG nominal voltage DC	72-96V
PVG open circuit voltage DC	200V
Solar generator [Wp]	350-1200
Max. motor current (A)	9.5
Pomp type	Centrifugal
Motor power	1.7kw
Motor rate	900-3300

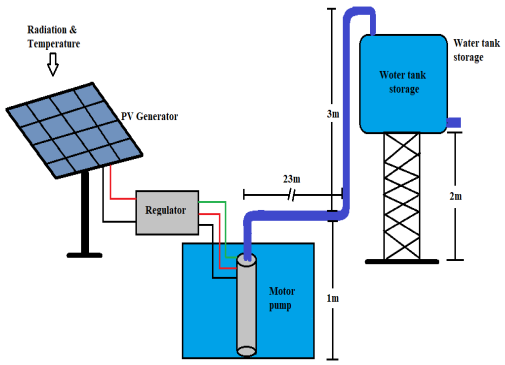

Fig. 1 The experimental setup

The system (Fig. 1) is used to fill a tank from the water source (an artificial lake) and operates only when the sun is shining. Instead of storing power in batteries, water is stored in the tank. Water tanks are far cheaper than battery banks and last for decades. Gravity is used to push stored water to the irrigation network. A low-water probe for dry-run protection is used, the purpose of such probe is to sense the loss of water and turn the pump off before it can run dry. To prevent overflow of the tank a float switch is used, this will stop the pump when the tank is full. Because the aim of this first study is to get the system performance at the studied area and not to irrigate, water was recycled into the lake.

The monitoring system ensures the measure of the electrical, hydraulic and climatic parameters. So the DC and AC parameters, voltage and current, were measured using two multimeters: BK precision 2880b multimeter and uni-t ut201 digital clamp multimeter. The water flow and pressure were measured respectively by water flow meter and a manometer. Air temperature and solar radiation were carried out using imetos station.

3. Pumping system modeling

This part gives the modeling of the PV panel, the controller, the BLDC motor and the centrifugal pump.

3.1 PVG system modeling

The equivalent circuit of a solar cell is shown in Fig.2. The main equation for the output current I_{pv} is (eq. 1) Zegaoui et al, (2011); Gupta & Jain (2013):

$$I_{pv} = I_{ph} - I_0\left(e^{\frac{q\left(V_{pv}+I_{pv}R_s\right)}{nkT}} - 1\right) - \frac{\left(V_{pv}+I_{pv}R_s\right)}{R_{sh}} \quad (1)$$

Where: I_{ph} is the photocurrent it is proportional to the solar irradiation flux; I_0 is the reverse saturation current of the diode; q is the electron charge ($1.602\text{x}10^{-19}$C); V_{pv} and I_{pv} are respectively the voltage and the current of the cell; R_s and R_{sh} are respectively the series and parallel resistance of the cell; n is known as the ideality factor of the diode; k is the Boltzmann's constant ($1.38\text{x}10^{-23}$ J/K); T is the junction temperature in Kelvin (K).

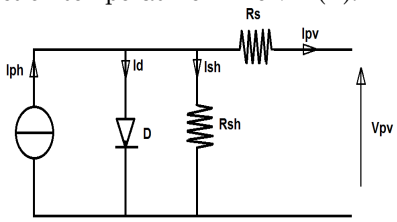

Fig. 2 Electrical model of the PV cell

The power generated by the PV module can be estimated by:

$$P_{pv} = I_{pv} \times V_{pv} \quad (2)$$

In order to obtain the current and voltage at MPP for a specific radiation and cell temperature, it is possible to differentiate the equation for power (eq.2) with respect to V_{pv} and set the result equal to zero. That's will increase the PV Panels efficiency which is expressed in the following equation (eq. 3), according to (Belgacem, 2012).

$$\eta = \frac{P_{pv}}{GA_{pv}} \quad (3)$$

Where G is the solar radiation and A_{pv} is the panels' surface.

3.2 Controller and BLDC motor modelling

The controller consists of a DC-DC chopper that ensures the MPPT and DC-AC inverter that provides the three phase voltage system needed by the BLDC (Fig. 3).

1) DC/DC converter

The DC/DC converter output voltage V_{dc} and load resistance R_L are respectively expressed in (eq. 4) and (eq. 5) Ba *et al*. (2018a, b).

$$V_{dc} = \alpha V_{pv} \quad (4)$$

$$R_L = \alpha^2 R_{pv} \quad (5)$$

Where α is the duty cycle ($0 \le \alpha \le 1$), R_{pv} is the PV generator resistor seen by the converter input.

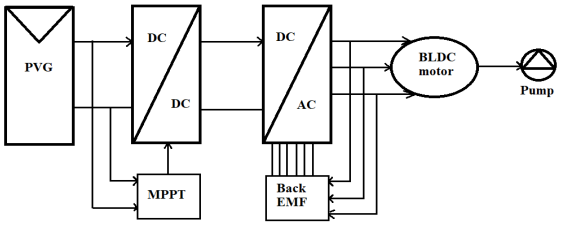

Fig. 3 Synoptic block of the water pumping system

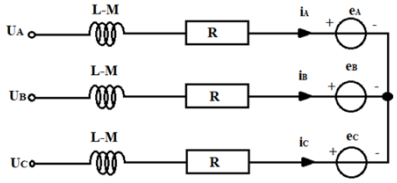

Fig. 4 Motor phases model

2) BLDC motor

Suppose that the three-phase BLDC motor as in (Fig. 4) is controlled by the full-bridge driving in the two-phase conduction mode. The state space model is in (eq. 6) (El-samahy & Shamseldin, 2016).

$$\begin{bmatrix} \dot{i}_A \\ \dot{i}_B \\ \dot{\Omega} \\ \dot{\theta}_m \end{bmatrix} = \begin{bmatrix} -R/L & 0 & 0 & 0 \\ 0 & -R/L & 0 & 0 \\ 0 & 0 & -B/J & 0 \\ 0 & 0 & 1 & 0 \end{bmatrix} \begin{bmatrix} i_A \\ i_B \\ \Omega \\ \theta_m \end{bmatrix} + \begin{bmatrix} 2/3L & 1/3L & 0 \\ -1/3L & 1/3L & 0 \\ 0 & 0 & 1/J \\ 0 & 0 & 0 \end{bmatrix} \begin{bmatrix} u_{AB}-e_{AB} \\ u_{BC}-e_{BC} \\ T_e-T_L \end{bmatrix} \quad (6)$$

3)DC/AC Inverter

Consider the interval when phases A and C are conducting and phase B is open as indicated by the shaded region Fig. 5. Phase A winding is connected to the positive terminal of the dc supply, phase C to the negative terminal of the dc supply and phase B is open. Therefore, $i_a = -i_c$ and $i_b = 0$. It can be seen from the shaded region that the back EMF in phases A and C are equal and opposite and the back EMF in phase B e_{bn} transits from one polarity to another crossing zero. Therefore in that interval u_{AB} - u_{BC} may be simplified as in (eq. 7).

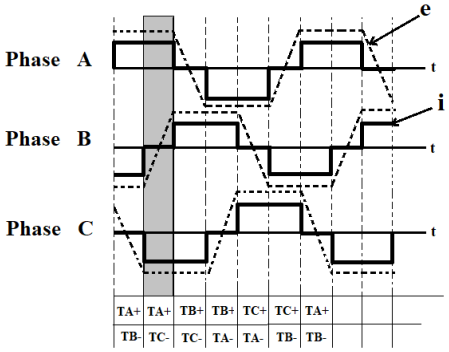

Fig. 5 Motor phases back EMF and current

$$u_{AB} - u_{BC} = e_{an} - 2e_{bn} - e_{cn} = -2e_{bn} \quad (7)$$

The difference of line voltages waveform is, thus, an inverted representation of the back EMF waveform and enables detection of the zero crossing of the phase B EMF. Therefore, the zero-crossing instants of the back EMF waveforms may be estimated indirectly from measurements of only the three terminal voltages of the motor. From the zero crossing of all the back EMF in a similar manner we obtain the switching sequence. Commutation instances are determined 30º from zero

crossing (Kavitha, Karthikeyan & Iswarya, 2004). The efficiency of the inverter is expressed by (eq.8).

$$\eta = \frac{P_{ac}}{P_{dc}} \quad (8)$$

3.3 Pump modelling

The pump represents the mechanical load of the BLDC motor, its flow-head characteristic can be expressed in quadratic form using Pfleiderer Peterman model (eq.9) (Al-Karaghouli & Al-Sabounchi, 2000). The total dynamic head can be expressed by (eq.10) (Kabade, Rajoriya & Chaubey, 2013). The hydraulic horse power (Ph) is done by (eq. 11) (Belgacem, 2012) and the load torque (TL) of the pump can be described by an aerodynamic load (eq. 12) (Kavitha, Karthikeyan & Iswarya, 2004):

$$TDH = \mu\Omega^2 - \lambda\Omega - \kappa Q^2 \quad (9)$$

$$TDH = Hg + \Delta H \quad (10)$$

$$Ph = \rho \times g \times TDH \times Q \quad (11)$$

$$T_L = a\Omega^2 \quad (12)$$

Where μ, λ and κ represent the geometric parameters characterizing the pump, Q (m^3/s) is the flow rate, Hg (m) is the static head, ΔH (m) is the total head loss, ρ (kg/m^3) is the water density, g (m/s^2) is the gravitational constant, a is the pump constant.

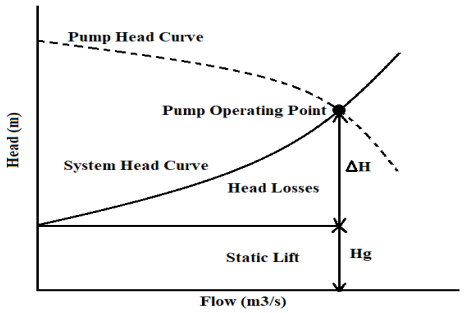

Fig. 6 typical pump curves

Fig. 6 illustrates the typical pump curves of a single impeller pump. It shows both the head-capacity curve of a centrifugal pump and the system curve. The operating point is the point at which the pump and system curves cross. The head loss is related to the square of the flow, and represents the resistance to the flow caused by pipe and equipment friction.

The subsystem (inverter, motor and pump) efficiency is the ration between the hydraulic power and the DC power (eq. 13).

$$\eta = \frac{P_h}{P_{dc}} = \frac{\rho \times g \times TDH \times Q}{P_{dc}} \quad (13)$$

4. Data analysis and results

The meteorological, electrical and hydraulic parameters were monitored hourly for four days. Table 3 shows the average value of the parameters. Throughout these days the PV panel was mounted at a tilt angle of 17° for the two first days and 7.5 for the two last days and oriented to magnetic North. The angle of 17° is approximately equal to the site's latitude and the angle of 7.5 was done to put the panel perpendicular to the sun's rays at noon.

Table 3
Parameters of the four studied days

Days number	01	02	03	04
Irradiation (kWh/m²/Day)	7.83	9.22	7.97	8.49
Temperature (°C)	29.52	33.03	40.22	29.06
Tilt angle (°)	17	17	7.5	7.5

4.1 Climatic parameters

The climatic parameters were monitored for one year. From table 4 we can see that the most shinning month is May, with a value of 8.26 kWh/m²/day, and the least shining months is January and December with respectively values of 3.00 and 3.35 kWh/m²/day. The medium value is 5.67 kWh/m²/day.

Table 4
Solar radiation per month

Month	Solar radiation (KWh/m²/day)
1	3,00
2	4,77
3	5,69
4	7,27
5	8,26
6	7,61
7	6,85
8	6,17
9	5,68
10	5,19
11	4,22
12	3,35

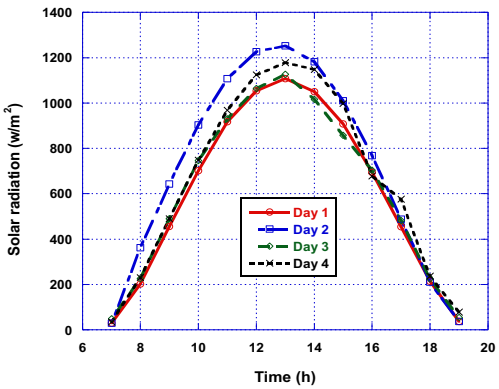

Fig. 7 Daily solar radiation versus time

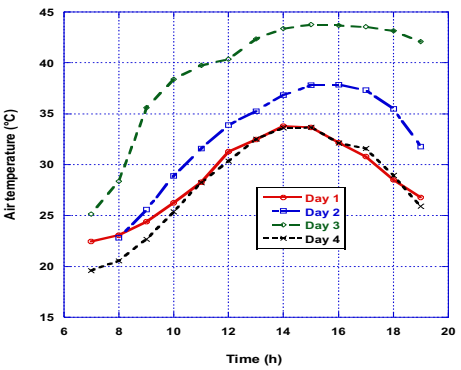

Fig. 8 Daily air temperature versus time

The Figures 7 and 8 show respectively the daily solar radiation and air temperature versus the time for four clear days (without clouds). The radiation pic arrives at 13 pm with a value of 1.2 kW/m² and the temperature varies from 20°C to 45°C. The average values of the radiation power and temperature are shown in Table 3 for these four days.

When the irradiation is less than 200 W/m² the PV modules do not generate enough energy to perfectly operate the pumping system and that occurs in the beginning of the day until 8am and in the end of the day after 6pm. So the electrical and hydraulic parameters were taken from 8am to 6pm corresponding to a total of 10 hours during the day.

4.2 PV panels simulations with MATLAB

Fig.9 and Fig. 10 represent the I-V characteristics of the PV generator respectively for six radiation levels from 200 W/m², considered as the minimum irradiance to run the system, to 1200 W/m2, considered as the maximum irradiance level present in the site (Rosso, southern Mauritania), at a fixed PV junction temperature (25°C) and for four PV junction temperature levels from 0°C to 75°C at a fixed radiation (1000 W/m²).

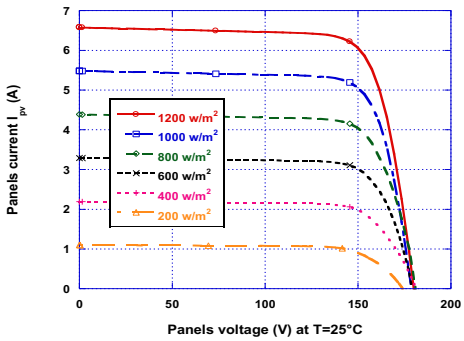

Fig. 9 I-V curves at different irradiations and constant temperature

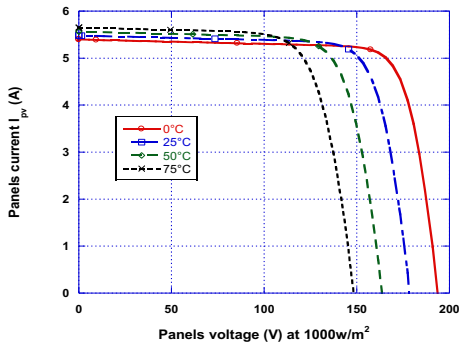

Fig. 10 I-V curves at different temperatures and constant irradiation

It is seen that the irradiation changes affect mainly the Panels current, while the temperature changes affect mainly the Panels voltage. Fig.11 and Fig. 12 represents the P-V characteristics of the PV generator respectively for the same six radiation levels at a fixed temperature (25°C) and for the same four temperature levels at a fixed radiation (1000 W/m²).

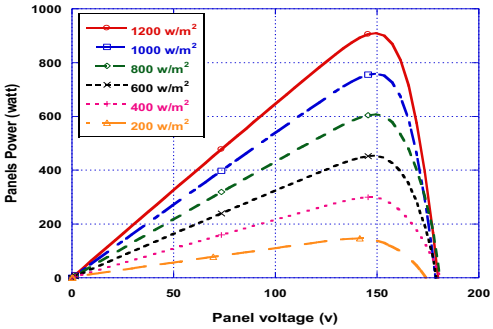

Fig. 11 P-V curves at different irradiations and constant temperature

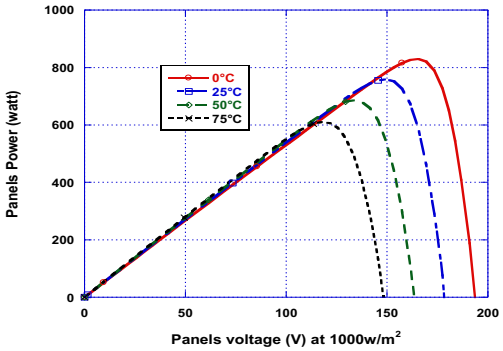

Fig. 12 P-V curves at different temperatures and constant radiation

They show the effect of varying weather conditions on the MPP. The PV Panels power increases as a consequence of the solar radiation increases or the temperature decreases. So we can plot the MPP versus radiation at a fixed temperature and versus temperature at a fixed radiation.

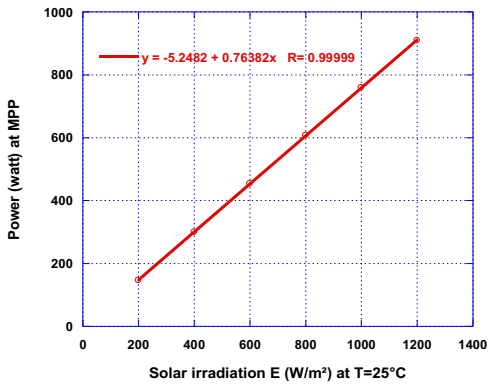

Fig. 13 MPP versus solar irradiations at constant temperature

Fig. 13 and Fig. 14 show respectively the curves of the power at the MPP versus radiation at a fixed junction temperature (25°C) and versus the junction temperature at a fixed radiation (1000 W/m²). We remark that the curve of the power at the MPP is linear in both cases versus radiation at a fixed temperature and versus temperature at a fixed radiation. The irradiation regression line has a sensibility of 763.82 W/(kW/m²). This linearity between the power at the MPP and radiation was also observed by Koutroulis, Kalaitzakis & Voulgaris, (2001); Hamrouni, Jraidi & Chérif, (2008). The temperature regression line has a sensibility of -2.94 W/°C.

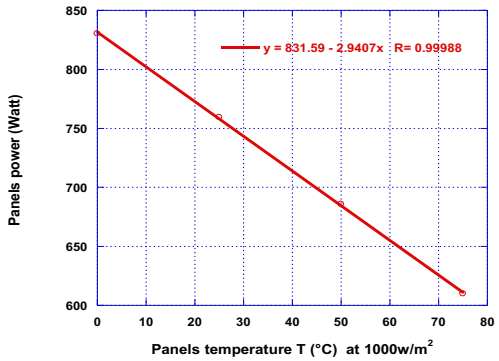

Fig. 14 MPP versus temperature at irradiation

But as we have seen in Fig.7 and Fig.8 radiation and temperature are varying at the same time in the course of the day. So how the MPP does varies through the day?. To answer this question a simulation was done by Matlab with a radiation and a temperature measured by the imetos station for four different days and the corresponding powers at the MPP were calculated.

Fig.15 shows the evolution of the power at the MPP versus time through the day for the four days. From that figure we observe that the power evolution is increasing and decreasing similar to radiation. We therefore plotted the power as a function of radiation, Figure 16, for the four days. And, we get linear curves with good regression for every day. The four regression lines show a sensibility variation from 593.02 W/(kW/m²) to 695.17 W/(kW/m²). Although the temperature changes through the days the power curves remain linear. This explains why the loss of power caused by the variation of temperature is neglected compared to that produced by the evolution of the radiation (Zhang, 2018).

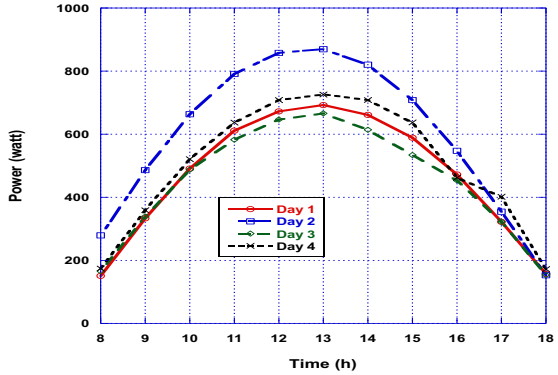

Fig. 15 MPP versus time

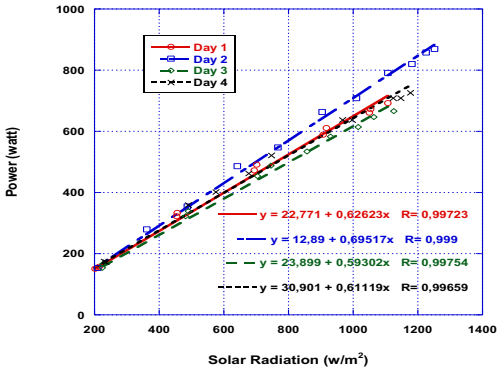

Fig. 16 MPP versus radiation

4.3 PV panels experimental results: Electrical DC parameters

The Solar panels voltage and current (DC parameters), system on, were measured every hours the corresponding power were calculated using (eq. 2). Figures 17 and 18 respectively show the evolution of the solar panels power versus time and irradiation. We remark that, the electrical power delivered by the panels under the MPPT algorithm is linear with the solar irradiation giving a good agreement with simulation and (Merino, Lagos & Gontupil, 2008). We can remark the difference between the values in simulation and in the experimental measurements, and that's because of the panels' degradation through the time. A regression line was added to each group of data.

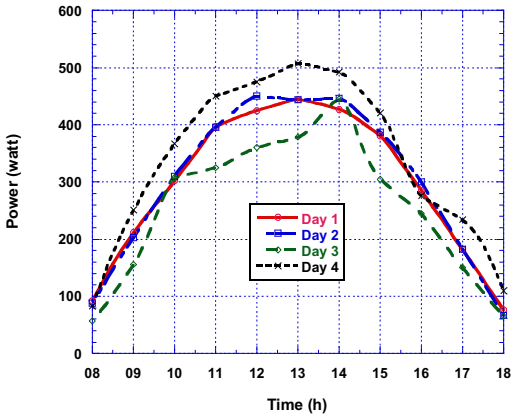

Fig. 17 Solar panels MPP versus time

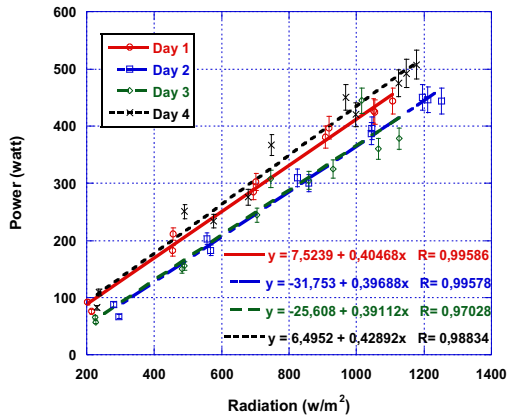

Fig. 18 Solar panels MPP versus radiation

The difference between the lines in figure 18 is linked to the difference of the day's temperatures. The four regression lines show a sensibility variation from 391.12 W/(kW/m²) to 428.92 W/(kW/m²). The electrical voltage depends on the temperature while the electrical current and power are mainly linked to the irradiation. This is due to the fact that Impp is not significantly affected by changes of the temperature and is directly related to radiation. According to equation (eq. 11) the PV Panels efficiency varies from 7.5 to 8.1%.

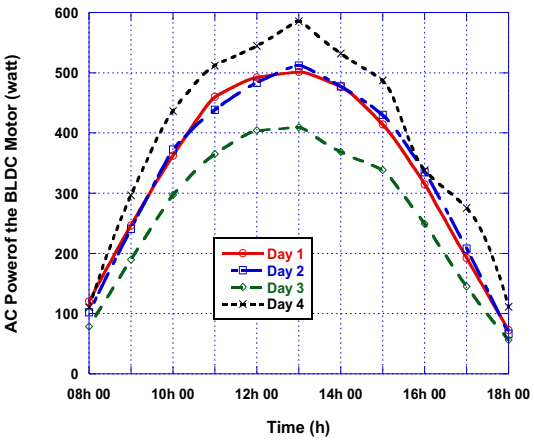

Fig. 19 Power of the BLDC motor versus time

4.4 controller experimental results: Electrical AC parameters

At any time only two phases are connected to the DC bus one of them is conducting in the positive direction and the other in the negative direction. The third phase is conducting in the freewheeling (Rao, Obulesh & Babu, 2012). The DC power delivered to the BLDC is divided between the two phases; meanwhile the AC power of the BLDC is the sum of the three phase's power. That explains why the BLDC power (Fig. 19) is higher than the DC power (Fig. 17). The efficiency of the inverter (eq.8) arrives to 120% increased by the freewheeling power.

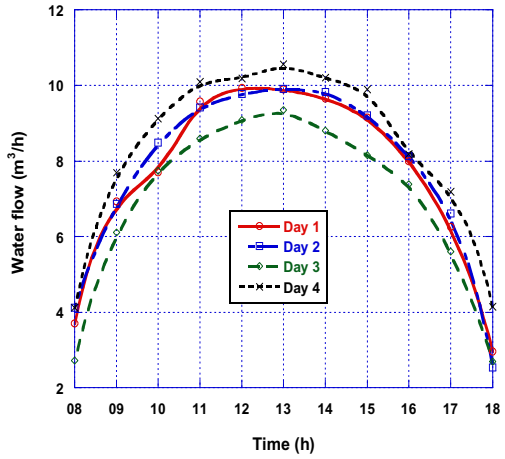

Fig. 20 Water flow versus time

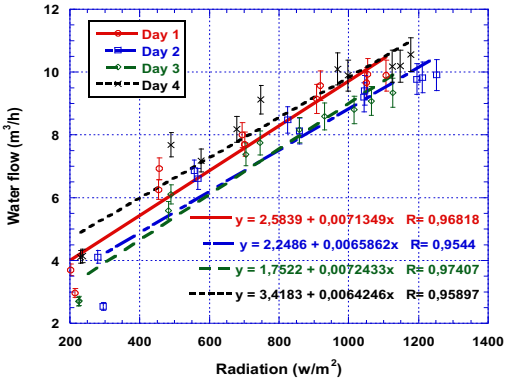

Fig. 21 Water flow versus radiation

4.5 Pump experimental results: hydraulic parameters

In Fig 20, we observe that the curves of the water flow versus time fellow the sunshine and the difference between them is linked to meteorological parameters, the picks arrives at 13h. In Fig. 21, we remark that the curves of the water flow versus irradiation are linear and the difference between them is linked to other parameters such temperature. The four regression lines shows a sensibility variation from 6.42 (m^3/h)/(kW/m^2) to 7.24 (m^3/h)/(kW/m^2). However in Fig 22, the curves of the water flow versus the DC power are linear and superimposed, with a value of the correlation coefficient more than 95%, confirming that the flow rate depends only on the power produced. The four regression lines shows a sensibility variation from 15 (m^3/h)/kW to 17.78 (m^3/h)/kW.

For a little head loss, the total pumping head TDH = H_g = 4m, so using (eq 13) the subsystem efficiency varies from 16 to 19% (water density ρ = 1000kg/m^3 and the gravitational constant g=9,81m/s^2).

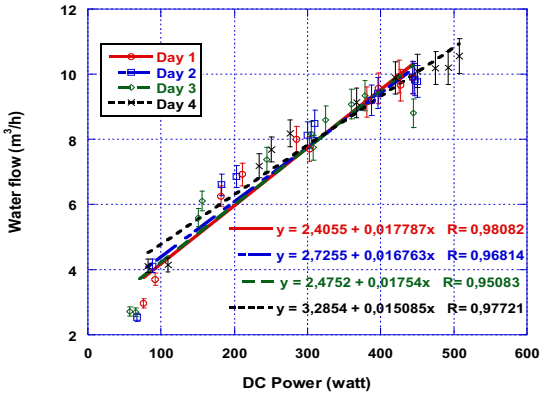

Fig. 22 Water flow versus DC Power

Integrating the water flow rate by time from Fig. 19, we found the water flow per day (Table 5) and we remark that the performances of the system increase with radiation and decreases with temperature.

Table 5
Water flow per day

Days number	01	02	03	04
Irradiation (kWh/m^2/Day)	7.83	9.22	7.97	8.49
Temperature (°C)	29.52	33.03	40.22	29.06
Tilt angle (°)	17	17	7.5	7.5
Water flow/day (m^3/day)	**83.79**	**84.88**	**76.25**	**91.40**

5. Conclusion

This system is suitable for many rural zones since it's designed to work with free cost and doesn't need maintenance. The maximum power point tracker device allows the system to overcome the mismatch between the load characteristics and the maximum power operation point of the PV module. The power and daily energy generated by the PV system gave a clear indication of the operational performance.

The monitoring of the weather condition shows that the most important radiation is in the month of May and the lowest is in the month of January. The pick of irradiation arrives at 13h and his value is more than 1200w/m^2. Simulations have proven the linearity between the MPP and radiation for the local climatic conditions. That

linearity was also confirmed by experimental measurement of the power delivered by the PV module under the MPPT algorithm. And the loss of power caused by temperature is neglected to that generated by radiation. The PV module efficiency varies from 6% to 8% and the subsystem efficiency (inverter, motor and pump) varies from 16% to 19%. We note that the AC power delivered by the BLCD motor is more important than the DC power because of the third phase conducting in the freewheeling. The water flow is linear with the DC power delivered by the PV module and by then is linear with the irradiation.

Here, we can notice that:

- ✓ The flow curve is symmetric around the pick value (10 m3/h) which arrives at 13pm.
- ✓ The solar pump starts at a solar radiation of 200w/m2 corresponding to a power of 100watt.
- ✓ For a power range from 0,1kw to 0,5kw we get a water flow range from 4 to more than 10m3/h. That corresponds to a sensibility of 15m3/h/kw.

In perspective this system would be very suitable to be applied on a small irrigation system where the need of water is 60 m^3/day. To guarantee a good use of water the irrigation should be controlled by a soil moisture sensor and equipped with a data logger system.

References

Abidin, Z., & Yesilata, B. (2004) New approaches on the optimization of directly coupled PV pumping systems, Solar Energy, 77 (1), 81-93.

Akbaba, M. (2006) Optimum matching parameters of an MPPT unit based for a PVG-powered water pumping system for maximum power transfer, Int. J. Energy Res., 30, 395–409.

Al-Karaghouli, A., & Al-Sabounchi, A.M. (2000) A PV pumping system, Applied Energy,65, 145-151.

Appelbaum, J., & Bany, J. (1979) Performance analysis of D.C. motor-photovoltaic converter system-I, Solar Energy, 22 (5),439-445.

Atlam, M.Y.O., & Kuyumcu, F. (2003) Application of genetic algorithms on a photovoltaic panel (PV)-pump motor matching to natural tracking of PV maximum power points, in Proc. Turkish Symp. Artificial Intelligence and Neural Networks, Canakkale, Turkey.

Ba, A., Aroudam, E., Chighali, O.E., Hamdoun, O., & Mohamed, M.L. (2018) Performance Optimisation of the PV pumping system, Procedia Manufacturing 22, 788-795.

Ba, A., Chighali, O.E., Mohamed El mamy, M.M., Hamdoun, O., & Aroudam, E. (2018) Comparative study of different DC/DC power converter for optimal PV system using MPPT (P&O) method, Applied Solar Energy, 54(4), 235-245.

Belgacem, B.G. (2012) Performance of submersible PV water pumping systems in Tunisia, Energy for Sustainable Development, 16, 415-420.

Calais, M., & Hinz, H. (1998) A ripple-based maximum power point tracking algorithm for a single-phase, grid-connected photovoltaic system, Solar Energy, 63(5), 277-282.

Chandel, S.S., Nagaraju, N.M., & Chandel, R. (2015) Review of solar photovoltaic water pumping system technology for irrigation and community drinking water supplies, Renewable and Sustainable Energy Reviews, 49, 1084–1099.

Elgendy, M.A., Zahawi, B., & Atkinson, D. J. (2010) Comparison of Directly Connected and Constant Voltage Controlled Photovoltaic Pumping Systems, IEEE Transactions on Sustainable Energy, 1(3), 184-192.

El-samahy, A.A., & Shamseldin, M.A. (2016) Brushless DC motor tracking control using self-tuning fuzzy PID control and model reference adaptive control, Ain Shams Engineering Journal 9(3), 341–352.

Fam, W. Z. & Balachander, M. K. (1988) Dynamic performance of a dc shunt motor connected to a photovoltaic array, IEEE Trans. Energy Convers., 3(3), 613–617.

Feraga, C.E., & Bouldjedri, A. (2016) Performance of a Photovoltaic Pumping System Driven by a Single Phase Induction Motor Connected to a Photovoltaic Generator, Automatika, 51, 163–172.

Gupta, M.K., & Jain, R. (2013) MPPT Simulation with DC Submersible Solar Pump using Output Sensing Direct Control Method and Cuk Converter, International Journal of Renewable Energy Research, 3 (1), 186-191.

Hadi, H., Tokuda, S., & Rahardjo, S. (2003) Evaluation of performance of photovoltaic system with maximum power point (MPP), Solar Energy Mater. Solar Cells, 75, 673–678.

Hadj Arab, A., Benghanem, M., & Chenlo, F. (2006) Motor-pump system modelization, Renewable Energy, 31,905–913.

Hamrouni, N., Jraidi, M. & Chérif, A., (2008) Solar radiation and ambient temperature effects on the performances of a PV pumping system, Revue des Energies Renouvelables, 11(1), 95–106.

Jain, A., Sarkar, P.R., & Siddique, M.K. (2015) Modeling and Performance Analysis of a Permanent Magnet Brushless DC motor using Instrumentation Technique, International Journal of Engineering Research and General Science, 3 (1), 814–820.

Kabade, A., Rajoriya, A., & Chaubey, U.C. (2013) Solar Pump Application in Rural Water Supply – A Case Study from Ethiopia, International of Energy Engineering, 3 (5), 176-182.

Kavitha, B., Karthikeyan, S., & Iswarya, B. (2004) Design of solar PV water pumping system using BLDC drive using sensorless method, The International Journal of Engineering and Science, 3 (3), 41-46.

Koner, P.K. (1995) Optimization techniques for a photovoltaic water pumping system, Renewable Energy, vol. 6, pp. 53–62.

Koutroulis, E., Kalaitzakis, K. & Voulgaris, N. (2001) Development of a Microcontroller-Based, Photovoltaic Maximum Power Point Tracking Control System, IEEE Transactions On Power Electronics, 16, 46–54.

Lawrance, B.W.W., & Langridge, D. (1995) Simulation and performance of a photovoltaic pumping system, in Proc. IEEE Int. Conf. Power Electronics and Drive Systems. 1,513–518.

Merino, G.G., Lagos, L.O., & Gontupil, J.E. (2008) Monitoring and evaluation of a direct coupled photovoltaic pumping system, Applied engineering in agriculture, 24 (3), 277-284.

Metwally H.M.B., & Anis, W.R. (1995) Performance analysis of photovoltaic pumping systems using switched reluctance motor drives, Progress in Photovoltaics, 3, 253–264.

Mustapha, T., Gauri, S., & Gürbüz, G. (2015) *Mauritania Renewebles, Readiness and Assessement,* International renewable Energy Agency, Abu Dhabi, United Arabe Emirates.

Rao, A.P.C., Obulesh, Y. P., & Babu, C.S. (2012) Mathematical modeling of BLDC motor with closed loop speed control using PID controller under various loading conditions, ARPN Journal of Engineering and Applied Sciences, 7, 1321-1328.

Roger, J.A. (1979) Theory of the direct coupling between D.C. motors and photovoltaic solar arrays, Solar Energy, 23 (3), 193-198.

Suehrcke, H., Appelbaum, J., & Reshef, B. (1997) Modelling a permanent magnet DC motor/centrifugal pump assembly in a photovoltaic energy system, Solar Energy, 59, 37–42.

Surendra, T.S., & Subbaraman, S.V.V. (2002) Solar PV water pumping comes of age in India, *in Proc. IEEE Photovoltaic Specialists Conf., pp. 1485–1488.*

Taha, M.S. & Suresh, K. (1996) Maximum power point tracking inverter for photovoltaic source pumping applications, in

Proc. IEEE Int. Conf. Power Electronics, Drives & Energy Systems for Industrial Growth, New Delhi, India, 2,883-886.

Vongmanee, V. (2004) The photovoltaic pumping system using a variable speed single phase induction motor drive controlled by field oriented principle, *in Proc. IEEE Asia-Pacific Conf. Circuits and Systems, Tainan, Taiwan, 2, 1185–1188.*

Whitfield, G.R., Bentley, R.W., & Burton, J. D. (1995) Increasing the cost effectiveness of small solar photovoltaic pumping systems, Renewable Energy, 6, 483–486.

Zegaoui, A., Aillerie, M., Petit, P., Sawicki, J.P., Jaafar, A., Salame, C., & Charles, J.P. (2011) Comparison of Two Common Maximum Power Point Trackers by Simulating of PV Generators, Energy Procedia 6, 678-687.

Zhang, Z. (2018) Influence of Special Weather on Output of PV System, IOP Conf. Series: Earth and Environmental Science, 108, 052063.